Borneo Journal of Pharmacy
Vol 7 Issue 3 August 2024
Pages 264 – 277

https://journal.umpr.ac.id/index.php/bjop/article/view/7218
DOI: https://doi.org/10.33084/bjop.v7i3.7218
e-ISSN: 2621-4814

Research Article

Affinity of Nintedanib Towards New Candidate Target for Idiopathic Pulmonary Fibrosis

Hari Baskar Balasubramanian [1]
Sima Biswas [2]
Maria Talmon [1]
Filippo Patrucco [3,4]
Piero Emilio Balbo [4]
Luigia Grazia Fresu [1*]
Angshuman Bagchi [2#]

[1] Department of Health Sciences, Università degli Studi del Piemonte Orientale "Amedeo Avogadro", Novara, Piedmont, Italy
[2] Department of Biochemistry and Biophysics, University of Kalyani, Kalyani, West Bengal, India
[3] Department of Translational Medicine, Università degli Studi del Piemonte Orientale "Amedeo Avogadro", Novara, Piedmont, Italy
[4] Department of Medical, Division of Respiratory Diseases, Azienda Ospedaliero Universitaria Maggiore della Carita, Novara, Piedmont, Italy

*email: luigia.fresu@med.uniupo.it; phone: +390321660687
#email: angshumanb@gmail.com; phone: +919051948843

Keywords:
ADMET-SAR properties
COACH server-binding site predictor
Idiopathic pulmonary fibrosis
Nintedanib

Abstract

Idiopathic pulmonary fibrosis (IPF) is a progressive disease due to aggregation of fibroblasts on lung parenchyma. Nintedanib, an indolinone-derived tyrosine kinase inhibitor (TKi) has been approved for the treatment of IPF and it is a well-known inhibitor of platelet-derived growth factor (PDGF) receptor-α and -β, fibroblast growth factor (FGF) receptor-1–3 and vascular endothelial growth factor (VEGF) receptor-1–3. This study aims to evaluate the binding interaction between new therapeutic protein candidates for IPF such as autotaxin, galectin-3, interleukin-13, chitotriosidase-1, JNK, RhoE-ROCK-1, ROCK-2 against nintedanib. In this investigation we predicted, computed, and analyzed the binding interactions of the drug nintedanib using an *in silico* approach called molecular docking. Our docking studies demonstrated that RhoE-ROCK1 and autotaxin showed strong binding affinities towards nintedanib compared to known targets such as VEGFR2 and FGFR1. We can therefore hypothesize a further contribution of nintedanib to the improvement of pathology due to its affinity towards new targets in the pathogenesis of IPF. The next step will be to evaluate the effects of this affinity *in vitro* on specific cellular models.

Received: February 16th, 2023
1st Revised: July 11th, 2023
2nd Revised: May 27th, 2024
Accepted: August 1st, 2024
Published: August 30th, 2024

© 2024 Hari Baskar Balasubramanian, Sima Biswas, Maria Talmon, Filippo Patrucco, Piero Emilio Balbo, Luigia Grazia Fresu, Angshuman Bagchi. Published by Institute for Research and Community Services Universitas Muhammadiyah Palangkaraya. This is an Open Access article under the CC-BY-SA License (http://creativecommons.org/licenses/by-sa/4.0/). DOI: https://doi.org/10.33084/bjop.v7i3.7218

INTRODUCTION

Idiopathic pulmonary fibrosis (IPF) is a progressive lung disease characterized by the accumulation of fibrotic tissue, leading to impaired gas exchange and ultimately respiratory failure[1]. Despite ongoing research, the precise molecular mechanisms underlying IPF development remain elusive[2]. A variety of factors have been implicated in IPF pathogenesis, including cigarette smoking, viral infections, chronic aspiration, exposure to environmental pollutants, genetic predisposition, and certain drugs[3]. The histopathological hallmark of IPF is the presence of fibroblast foci, where myofibroblasts and excessive collagen deposition contribute to the distortion of lung architecture[1]. Alveolar macrophages play a pivotal role in initiating

How to cite: Balasubramanian HB, Biswas S, Talmon M, Patrucco F, Balbo PE, Fresu LG, et al. Affinity of Nintedanib Towards New Candidate Target for Idiopathic Pulmonary Fibrosis. Borneo J Pharm. 2024;7(3):264-77. doi:10.33084/bjop.v7i3.7218

the fibrotic process by secreting proinflammatory and profibrotic cytokines that stimulate mesenchymal cell proliferation and collagen deposition[4,5].

Currently, only two drugs, pirfenidone[6] and nintedanib[7], are approved for IPF treatment. While these medications can slow disease progression as measured by forced vital capacity (FVC), they do not reverse the fibrotic tissue changes observed on high-resolution computed tomography (CT) scans. Consequently, they often fail to improve disease-related symptoms and quality of life for IPF patients[3]. Ongoing research efforts are focused on developing novel therapeutic approaches targeting various pathways involved in IPF pathogenesis. These include new drug delivery systems and molecules that act on distinct mechanisms[8,9].

Nintedanib, a tyrosine kinase inhibitor, targets platelet-derived growth factor (PDGF), fibroblast growth factor (FGF), and vascular endothelial growth factor (VEGF) receptors, inhibiting their intracellular signaling by competitively binding to the ATP-binding site[10]. While nintedanib has demonstrated efficacy in treating idiopathic pulmonary fibrosis (IPF), this study aimed to explore its potential interactions with additional proteins implicated in IPF pathogenesis. Specifically, we investigated the binding affinity of nintedanib to RhoE-ROCK1, c-Jun N-terminal kinase (JNK), interleukin (IL)-13, human galectin-3 (Gal-3), autotaxin, human chitotrosidase-1 (CHIT-1) and the Rho-associated protein kinase-2 (ROCK2). These proteins have been implicated in the development or progression of IPF[8], suggesting that their modulation might offer therapeutic benefits.

Autotaxin, an enzyme responsible for lysophosphatidic acid (LPA) production, plays a crucial role in IPF by promoting fibroblast migration and inducing apoptosis of lung epithelial cells. Elevated levels of autotaxin and LPA have been observed in the bronchoalveolar lavage fluid and exhaled breath of IPF patients[11-14]. Targeting autotaxin could potentially mitigate the fibrotic process in IPF.

Galectin-3, a lectin involved in fibrosis, regulates the expression of transforming growth factor beta (TGF-β) receptors and has been found to be elevated in IPF patients[15]. The Rho-ROCK pathway, implicated in IPF fibrosis, is activated by oxidative stress and plays a role in regulating the cytoskeleton and cell motility[16]. Targeting the Rho-ROCK pathway has shown promise in reducing fibrosis in preclinical models[16-18].

Interleukin-13, a pro-fibrotic cytokine, is involved in asthma and has been associated with IPF pathogenesis[19-22]. While IL-13 inhibitors have shown efficacy in asthma, their effectiveness in IPF is limited. However, the combination of pirfenidone and lebrikizumab has demonstrated positive effects in reducing exacerbations in IPF patients[23].

Chitotrosidase-1, an enzyme involved in chitin degradation, has been implicated in fibrosis by modulating TGF-β and IL-13 signaling[24,25]. Targeting CHIT-1 has shown promise in reducing fibrosis in preclinical models[26]. Finally, the JNK pathway, involved in inflammation and fibrosis, is activated in IPF and has been shown to contribute to the fibrotic process[27,28]. JNK inhibitors have demonstrated efficacy in reducing fibrosis in preclinical models[29,30].

Existing literature lacks studies investigating the molecular interactions between nintedanib and ancillary proteins implicated in IPF. To address this knowledge gap, we employed molecular docking to predict and analyze the binding interactions of nintedanib with these proteins. By identifying potential alternative targets, this study aims to elucidate the mechanisms underlying nintedanib's efficacy and explore avenues for developing novel therapeutic strategies.

MATERIALS AND METHODS

Materials

The three-dimensional (3D) structures of target proteins, including RhoE-ROCK1 (PDB ID: 2V55), JNK (PDB ID: 3V6R), IL-13 (PDB ID: 4I77), human Gal-3 (PDB ID: 5H9P), autotaxin (PDB ID: 6W35), human CHIT-1 (PDB ID: 6Z8E), and ROCK2 (PDB ID: 7JNT), were retrieved from the Protein Data Bank (PDB). Additionally, the structures of VEGFR2 (PDB ID: 3C7Q) and chain A and B of FGFR1 (PDB ID: 1FGK) were obtained for use as positive controls, as nintedanib is known to bind these proteins. The 3D structure of the ligand nintedanib (PubChem CID: 135423438) was retrieved from the PubChem database. A summary of the software, web servers, and databases used in this study is provided in **Table I**.

Table I. The software, web servers, and databases used.

Software	link
Discovery Studio 2.5	Standalone version; Dassault Systèmes, Vélizy-Villacoublay, France
AutoDock 4.0	Standalone version; The Scripps Research Institute, La Jolla, CA, US
COACH Server	https://zhanggroup.org/COACH/
LigPlot+	https://www.ebi.ac.uk/thornton-srv/software/LigPlus/
Lipinski Filter	http://www.scfbio-iitd.res.in/software/drugdesign/lipinski.jsp
AdmetSAR server	http://lmmd.ecust.edu.cn/admetsar2
PubChem	https://pubchem.ncbi.nlm.nih.gov/
PDB	https://www.rcsb.org/

Methods

Preparation of receptor and ligand structures

Co-crystallized molecules and crystallographic water molecules were removed from the three-dimensional coordinate files using Discovery Studio Visualizer 2.5. This step was necessary to ensure that the protein structures were free of extraneous molecules for accurate docking calculations[31]. Subsequently, the protein structures were geometrically optimized using Discovery Studio Visualizer 2.5, employing a standard energy minimization protocol to alleviate steric clashes and bond distortions. The ligand molecule was also optimized using the same software and protocol.

Prediction of active sites

Accurate identification of a protein's active site is crucial in *de novo* drug design and molecular docking approaches. This knowledge facilitates the generation of near-native conformations for the receptor-ligand complex, ultimately contributing to the success of the docking study[32]. Here, the COACH server was employed to predict the active site amino acid residues for all target proteins[33]. Additionally, the active site residues of VEGFR2 and FGFR1 were retrieved from the literature for comparison.

Molecular docking analysis

A molecular docking study was performed using the AutoDock 4 software suite. AutoDock employs a Lamarckian genetic algorithm to predict the binding orientation and affinity of small molecules (ligands) to macromolecules (receptors)[34]. Ligand structures were prepared using Discovery Studio Visualizer 2.5. Polar hydrogen atoms were added, Kollman united atom type charges were assigned, fragmental volumes were calculated, and solvation parameters were set using AutoDockTools. These parameters were saved for subsequent docking simulations.

Binding site information for each ligand-receptor complex was identified using the COACH server and incorporated into AutoDock[33]. AutoGrid was utilized to generate a grid map encompassing the binding site residues of the receptor protein. This grid-based approach optimizes computational efficiency and improves docking accuracy. Lamarckian genetic algorithm searches were performed for each ligand-receptor complex using AutoDock. Each docking simulation yielded ten unique ligand conformations within the defined binding site.

Prediction of the physiochemical properties of the ligand

To assess the drug-like properties of nintedanib, we employed the admetSAR server and the Lipinski rule of five[28]. The Lipinski rule of five is a set of guidelines used to evaluate a ligand's potential for oral bioavailability. The admetSAR server provides a user-friendly interface to visualize various physiochemical and pharmacological properties of ligands relevant to drug discovery, including LogP (octanol-water partition coefficient), hydrogen bond donor and acceptor count, molecular weight, and rotatable bond count. These properties are crucial factors influencing a ligand's potential as a drug candidate. The admetSAR server was used to assess the combined effects of these properties, along with pharmacokinetics and pharmacodynamics, and generate a drug-likeness score.

Data analysis

The Discovery Studio Visualizer 2.5 was employed to visualize the interactions between the receptor and ligand within the protein-ligand complexes. LigPlot+, a web-based tool, was used to analyze the binding interaction profile in detail. This tool calculates the various non-covalent interactions (e.g., hydrogen bonds, hydrophobic interactions) established between the ligand and the receptor.

RESULTS AND DISCUSSION

Analysis of the active sites of the receptor

Amino acid residues within the active sites of proteins play crucial roles in ligand binding interactions. Understanding these interactions is vital for drug discovery and protein-ligand docking studies[35]. We employed the COACH server to predict potential ligand binding sites using the amino acid sequences and structural information of the receptor proteins. The results of these analyses are presented in **Tables II** to **VII**. Given the diverse methodologies employed by the various tools within the COACH server, we adopted a consensus approach to analyze the results. By considering the outputs from all tools, we aimed to identify consistent predictions regarding potential ligand binding sites. The consensus amino acid residues present in the binding site of the proteins were used for docking purposes. We used the method of directed docking by specifying the amino acid residues of the ligand proteins, by looking for amino acid residues that always appear in the results of each test parameter (COACH server, TM SITE, S-SITE, and COFACTOR). The results show that there are 8, 9, 7, 10, 9, and 8 consensus amino acids in CHIT-1, ROCK2, Gal-3, RhoE-ROCK1, JNK, and autotaxin, respectively.

Table II. COACH server results of human CHIT-1 (PDB ID: 6Z8E).

Parameter	Amino acid residues
COACH server	TYR27, PHE58, GLY98, TRP99, ASP138, GLU140, ALA183, MET210, TYR212, ASP213, TYR267, TRP358
TM SITE	TYR27, PHE58, GLY98, TRP99, ASP138, GLU140, ALA183, MET210, TYR212, ASP213, TYR267, ARG269, TRP358
S-SITE	TYR27, TRP31, PHE58, GLY98, TRP99, ASN100, ASP138, GLU140, TYR141, ALA183, MET210, TYR212, ASP213, TRP218, TYR267, ARG269, GLU297, MET300, MET356, TRP358, ALA359, LEU362
COFACTOR	TYR27, TRP31, PHE58, GLY98, TRP99, ASN100, PHE101, ASP138, GLU140, TYR141, ALA183, MET210, TYR212, ASP213, TYR267, ARG269, GLU297, MET300, TRP358, LEU362
Consensus binding site	TYR27, TRP99, ASP138, GLU140, MET210, TYR212, ASP213, TRP358

Table III. COACH server results of ROCK2 (PDB ID: 7JNT).

Parameter	Amino acid residues
COACH server	ILE98, GLY99, ARG100, GLY101, ALA102, VAL106, ALA119, LYS121, VAL153, MET169, GLU170, TYR171, MET172, PRO173, GLY175, ASP218, ASN219, LEU221, ALA231, ASP232
TM SITE	ILE98, GLY99, ARG100, GLY101, VAL106, ALA119, LYS121, GLU140, VAL153, MET169, GLU170, TYR171, MET172, PRO173, GLY175, ASP176, ASP218, LEU221, ALA231, ASP232
S-SITE	ILE98, GLY99, ARG100, GLY101, ALA102, PHE103, GLY104, VAL106, ALA119, LYS121, GLU140, VAL153, MET169, GLU170, TYR171, MET172, PRO173, GLY174, GLY175, ASP176, ASN179, ASP218, ASN219, LEU221, ALA231, ASP232
COFACTOR	ILE98, VAL106, ALA119, LYS121, VAL153, MET169, GLU170, TYR171, MET172, ASP218, ASN219, LEU221, ASP232, VAL372
Consensus binding site	ILE98, VAL106, ALA119, LYS121, VAL153, MET169, MET172, LEU221, ASP232

Table IV. COACH server results of Gal-3 (PDB ID: 5H9P).

Parameter	Amino acid residues
COACH server	HIS158, ASN160, ARG162, ASN174, TRP181, GLU184, ARG186
TM SITE	HIS158, ASN160, ARG162, VAL172, ASN174, TRP181, GLU184, ARG186
S-SITE	ARG144, ALA146, HIS158, ASN160, ARG162, GLU165, VAL172, ASN174, TRP181, GLU184, ARG186
COFACTOR	ARG144, HIS158, ASN160, ARG162, GLU165, ASN174, TRP181, GLU184, ARG186
Consensus binding site	HIS158, ASN160, ARG162, ASN174, TRP181, GLU184, ARG186

Table V. COACH server results of RhoE-ROCK1 (PDB ID: 2V55).

Parameter	Amino acid residues
COACH server	ILE82, GLY83, ARG84, GLY85, VAL90, ALA103, LYS105, VAL137, MET153, GLU154, TYR155, MET156, GLY159, ASP160, ASP202, ASN203, LEU205, ALA215, ASP216
TM SITE	LYS80, ILE82, GLY83, ARG84, GLY85, VAL90, ALA103, LYS105, MET153, GLU154, TYR155, MET156, PRO157, GLY159, ASP160, ASP202, ASN203, LEU205, ALA215, ASP216
S-SITE	ILE82, GLY83, ARG84, GLY85, ALA86, PHE87, GLY88, VAL90, ALA103, LYS105, VAL137, MET153, GLU154, TYR155, MET156, PRO157, GLY158, GLY159, ASP160, ASN163, ASP202, ASN203, LEU205, ALA215, ASP216
COFACTOR	ILE82, GLY83, ARG84, GLY85, GLY88, GLU89, VAL90, ALA103, LYS105, VAL137, MET153, GLU154, MET156, ASP202, LEU205, ALA215, ASP216
Consensus binding site	ILE82, GLY83, GLY85, VAL90,ALA103, LYS105, MET153, MET156, LEU205, ALA215, ASP216

Table VI. COACH server results of JNK (PDB ID: 3V6R).

Parameter	Amino acid residues
COACH server	ILE70, GLY71, SER72, VAL78, ALA91, LYS93, ILE124, MET146, GLU147, LEU148, MET149, ASP150, ALA151, ASN152, SER193, ASN194, VAL196, LEU206, ASP207
TM SITE	ILE70, GLY71, VAL78, ALA91, LYS93, ILE124, MET146, GLU147, LEU148, MET149, ASP150, ALA151, ASN152, SER193, ASN194, VAL196, LEU206, ASP207
S-SITE	ILE70, GLY71, SER72, GLY73, GLN75, GLY76, VAL78, ALA91, LYS93, GLJU111, MET115, ILE124, LEU144, MET146, GLU147, LEU148, MET149, ASP150, ALA151, ASN152, GLN155, SER193, ASN194, VAL196, LEU206, ASP207, PHE208
COFACTOR	VAL78, ALA91, LYS93, ARG107, GLU111, ILE124, LEU144, MET146, MET149, ASP150, ALA151, GLN155, LEU206, ASP207
Consensus binding site	VAL78, ALA91, LYS93, ILE124, MET149, ASP150, ALA151, LEU206, ASP207

Table VII. COACH server results of autotaxin (PDB ID: 6W35).

Parameter	Amino acid residues
COACH server	ILE168, ASP172, LYS209, THR210, PHE211, LEU217, ALA218, ASN231, PHE274, PHE275, TYR307, ASP312, HIS316, HIS475, MET513
TM SITE	ILE168, ASP172, LYS209, THR210, PHE211, LEU217, ALA218, ASN231, PHE274, PHE275, TYR307, ASP312, HIS316, HIS475, MET513
S-SITE	ILE168, SER170, ASP172, LYS209, THR210, PHE211, LEU214, LEU217, ALA218, ASN231, LEU244, TRP255, TRP261, PHE274, PHE275, ALA305, TYR307, ASP312, HIS316, ASP359, HIS360, HIS475, MET513
COFACTOR	ILE168, SER170, THR210, PHE211, LEU214, ALA218, ILE228, ASN231, LEU244, TRP255, TRP261, PHE274, ALA305, TYR307, ASP312, HIS316, HIS475
Consensus binding site	THR210, PHE211, ALA218, ASN231, TYR307, ASP312, HS316, HIS475

Molecular docking simulations (Site-specific and blind docking)

Molecular docking simulations were conducted using AutoDock 4.0 to predict the binding interactions between nintedanib and the target proteins. AutoDock 4 employs a genetic algorithm for docking simulations, generating a set of potential protein-ligand complex conformations. These conformations were ranked based on their binding free energy values, with those exhibiting the most favorable binding energies selected for further analysis (**Table VIII**). Given the known amino acid residues involved in nintedanib binding, site-directed docking was employed for these proteins. For other proteins where binding site information was unavailable, both blind and site-specific docking simulations were performed.

For each receptor protein, two sets of docking experiments were performed: site-specific (directed) and blind docking. Directed docking utilized previously identified binding site information to constrain the ligand's search space. In contrast, blind docking allowed the ligand to explore the entire receptor protein surface to identify the most favorable binding site. This dual approach provided a more comprehensive assessment of potential binding interactions[36].

The binding free energy values obtained from both docking methods were analyzed to identify the most promising binding conformations. LigPlot+ was used to visualize the binding interactions between the ligand and the receptor proteins. While the COACH server could not identify specific binding sites for IL-13, we conducted blind docking simulations for this molecule. As nintedanib's binding sites on VEGFR2 and FGFR1 are well-established, control experiments did not involve blind docking for these receptors. Our prime focus in this study is to check the interaction pattern of the Nintedanib with the following proteins RhoE-ROCK1, JNK, IL-13, Gal-3, autotaxin, CHIT-1, and ROCK2, therefore the co-crystal/reference ligands were removed from their structures. While nintedanib displayed favorable binding affinities for all target proteins, RhoE-ROCK1, CHIT-1, and JNK emerged as the most promising targets based on their binding free energy values. As detailed in **Table IX**, we employed the following docking protocols for each protein. The binding interactions between nintedanib and these receptor proteins are depicted in **Figures 1** and **2**.

Table VIII. Binding free energy from docking results.

Receptors	Binding free energy (kcal/mol)	
	Site-specific docking	Blind docking
VEGFR2	-9.27	-
FGFR1 (ChainA)	-8.74	-
FGFR1 (ChainB)	-6.17	-
Autotaxin (6W35)	-11.45	-5.00
RhoE-ROCK1 (2V55)	-11.57	-8.26
JNK (3V6R)	-8.60	-6.87
CHIT-1 (6Z8E)	-8.30	-8.98
ROCK2 (7JNT)	-5.45	-8.90
Gal-3 (5H9P)	-4.69	-6.49
IL-13 (4I77)	-	-5.46

Table IX. Binding free energy from docking results.

Protein ID	Parameters	Site-specific docking	Blind docking
2V55	Grid Points(user specific)	X-points: 58	X-points: 126
		Y-points: 52	Y-points: 126
		Z-points: 82	Z-points: 126
	Central Grid point of maps	(-15.787, 46.861, 34.694)	(-31.351, 48.495, 19.430)
	Macromolecule file in Grid maps	2V55NEW.pdbqt	2V55.pdbqt
	Grid parameter file	2V55.gpf	2V55.gpf
	Minimum Coordinates in grids	(-27.155, 36.669, 18.622)	(-82.948, -3.102, -32.167)
	Maximum Coordinates in grids	(-4.419, 57.053, 50.766)	(20.246,100.092, 71.027)
3V6R	Grid Points (user specific)	X-points: 74	X-points: 126
		Y-points: 46	Y-points: 126
		Z-points: 98	Z-points: 126
	Central Grid point of maps	(16.554, -15.429, -23.232)	(21.633, -22.936, -18.874)
	Macromolecule file in Grid maps	3V6Rnew.pdbqt	3V6Rnew.pdbqt
	Grid parameter file	3V6R.gpf	3V6R.gpf
	Minimum Coordinates in grids	(2.679, -24.054, -41.607)	(-14.970, -59.539, -55.477)
6Z8E	Grid Points (user specific)	X-points: 60	X-points: 126
		Y-points: 30	Y-points: 126
		Z-points: 26	Z-points: 126
	Central Grid point of maps	(8.954, -2.708, -10.629)	(14.600, -4.887, -10.506)
	Macromolecule file in Grid maps	6Z8ENEW.pdbqt	6Z8E.pdbqt
	Grid parameter file	6Z8E.gpf	6Z8E.gpf
	Minimum Coordinates in grids	(-14.626, -14.498, -20.847)	(-16.018,-35.505, -41.124)
7JNT	Grid Points (user specific)	X-points: 28	X-points: 126
		Y-points: 28	Y-points: 126
		Z-points: 22	Z-points: 126
	Central Grid point of maps	(48.025, 60.570, 42.725)	(46.477, 73.347, 44.105)
	Macromolecule file in Grid maps	7JNTNEW.pdbqt	7JNT.pdbqt
	Grid parameter file	7JNT.gpf	7JNT.gpf
	Minimum Coordinates in grids	(34.025, 46.570, 31.725)	(6.409, 36.459, 4.037)
5H9P	Grid Points (user specific)	X-points: 48	X-points: 110
		Y-points: 36	Y-points: 120
		Z-points: 54	Z-points: 116
	Central Grid point of maps	(-19.226, 4.508, 1.724)	(-13.132, -0.460, 6.424)
	Macromolecule file in Grid maps	5H9Pnew.pdbqt	5H9P.pdbqt
	Grid parameter file	5H9P.gpf	5H9P.gpf
	Minimum Coordinates in grids	(-29.162, -2.944, -9.454)	(-33.757, -22.960, -15.326)
6W35	Grid Points (user specific)	X-points: 64	X-points: 126
		Y-points: 56	Y-points: 126
		Z-points: 80	Z-points: 126
	Central Grid point of maps	(16.142, 3.060, 20.584)	(-4.699, 3.083, 17.187)
	Macromolecule file in Grid maps	6W35new.pdbqt	6w351.pdbqt
	Grid parameter file	6W35.gpf	6w351.gpf
	Minimum Coordinates in grids	(4.142, -7.440, 5.584)	(-66.124, -58.342, -44.238)
4I77	Grid Points (user specific)	Not performed as no data for the binding sites were found from the COACH server	X-points: 126
			Y-points: 90
			Z-points: 100
	Central Grid point of maps		(0.775, 31.603, -24.165)
	Macromolecule file in Grid maps		4I771.pdbqt
	Grid parameter file		4I771.gpf
	Minimum Coordinates in grids		(-62.225, -13.397, -74.165)
1FGK (Chain-A)	Grid Points (user specific)	X-points: 74	Not performed
		Y-points: 82	
		Z-points: 126	
	Central Grid point of maps	(3.900, 6.729, 17.631)	
	Macromolecule file in Grid maps	FGK1.pdbqt	
	Grid parameter file	FGK1.gpf	
	Minimum Coordinates in grids	(-6.941, -5.284, -0.828)	
1FGK (Chain-B)	Grid Points (user specific)	X-points: 60	Not performed
		Y-points: 114	
		Z-points: 102	
	Central Grid point of maps	(70.806, 4.003, 15.899)	
	Macromolecule file in Grid maps	FGK1.pdbqt	
	Grid parameter file	FGK1.gpf	
	Minimum Coordinates in grids	(62.016, -12.698, 0.956)	
3C7Q	Grid Points (user specific)	X-points: 94	Not performed
		Y-points: 126	
		Z-points: 82	
	Central Grid point of maps	(20.635, 59.454, 37.551)	
	Macromolecule file in Grid maps	VEGFR2.pdbqt	
	Grid parameter file	VEFGFR2.gpf	
	Minimum Coordinates in grids	(8.509, 43.200, 26.973)	

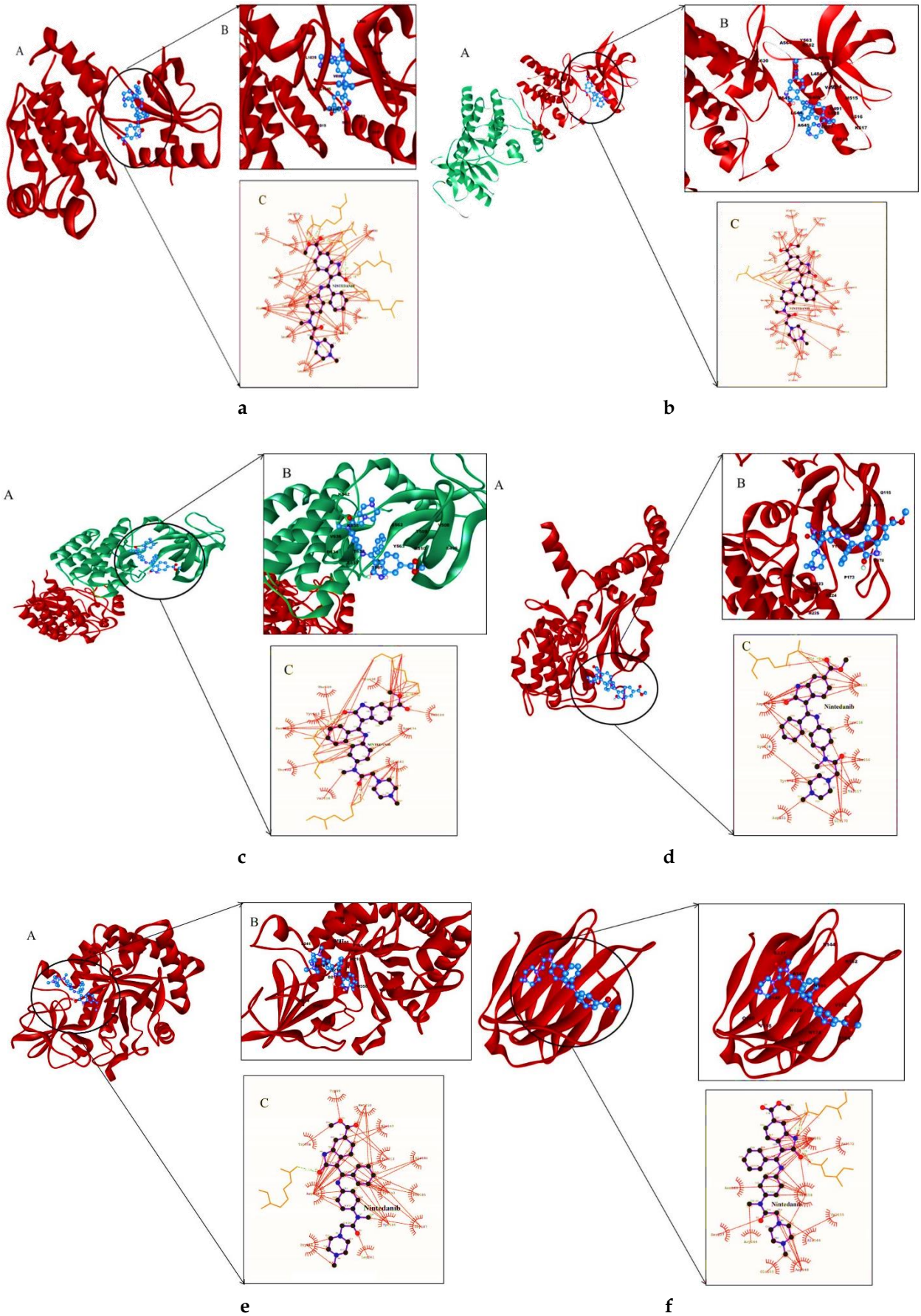
A
B
C
a
b
c
d
e
f
Nintedanib

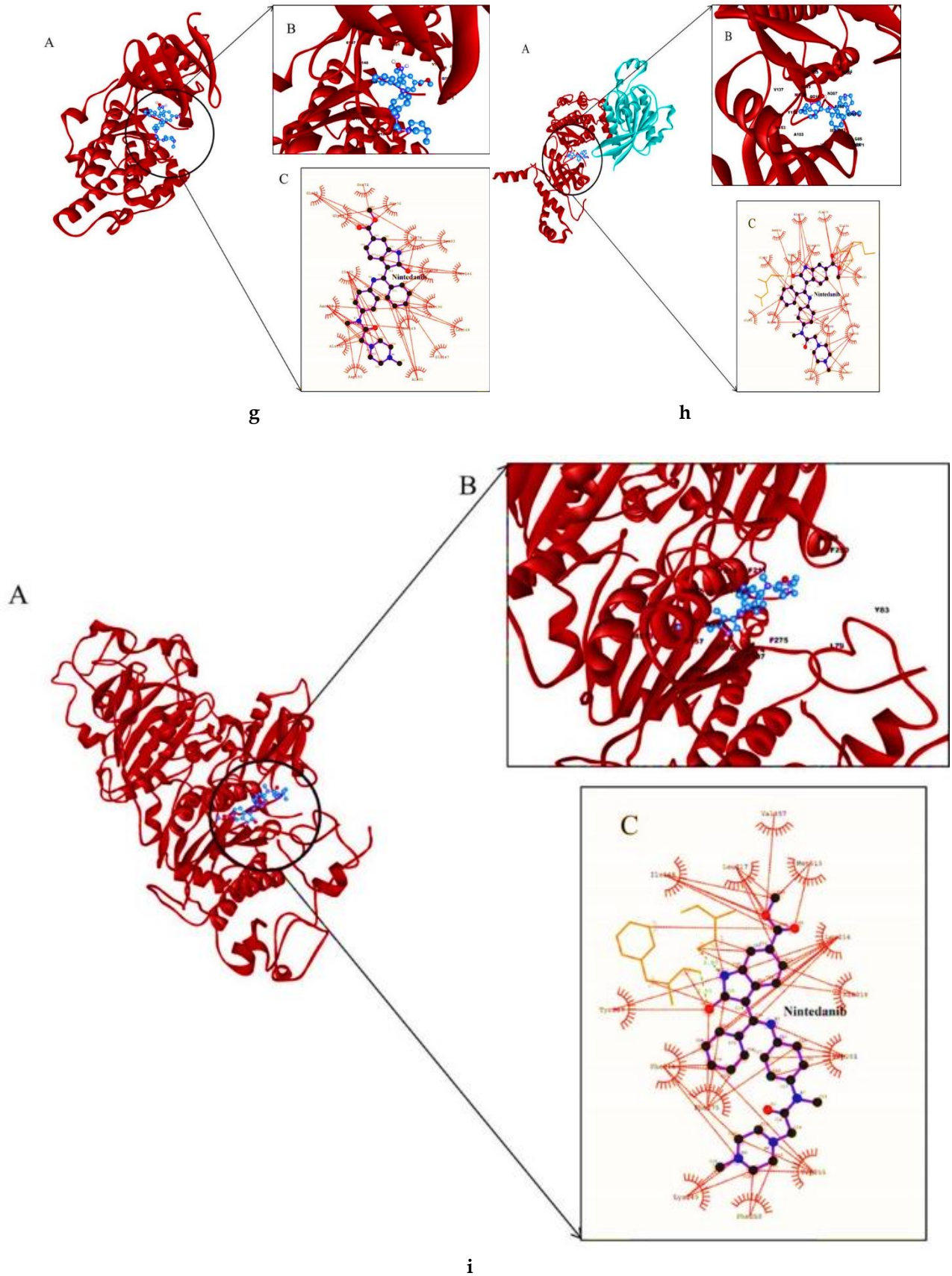

Figure 1. The binding interactions between the ligand and the different protein receptors (site-specific) of **a**: VEGFR2; **b**: FGFR1 Chain-A; **c**: FGFR1 Chain-B; **d**: ROCK2; **e**: CHIT-1; **f**: Gal-3; **g**: JNK; **h**: RhoE-ROCK1; and **i**: autotaxin. In each panel, **A-** represents the binding of the ligand with the receptor protein (the receptor protein is represented in the cartoon. The ligand is presented in ball stick model). **B-** represents the amino acid residues of the receptor protein binding with the ligand. **C-** represents the various types of non-covalent interactions during the binding of the ligand with the receptor.

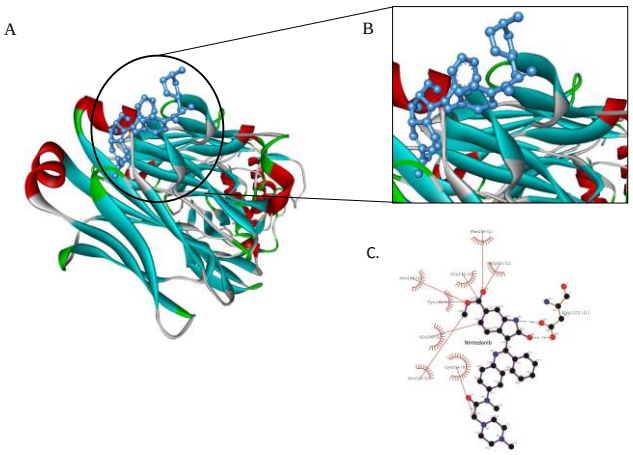
A
B
C.
Nintedanib

a

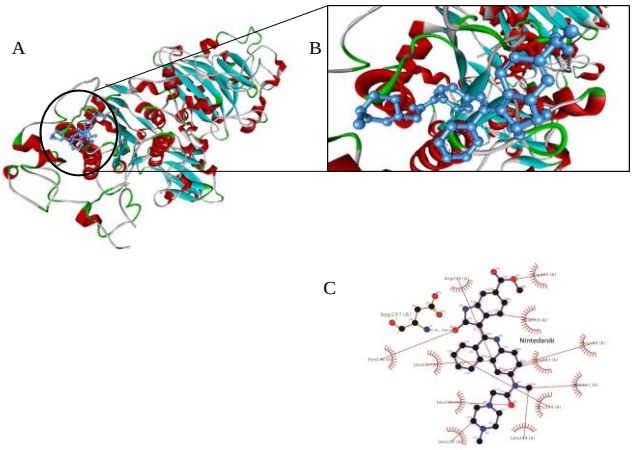
A
B
C
Nintedanib

b

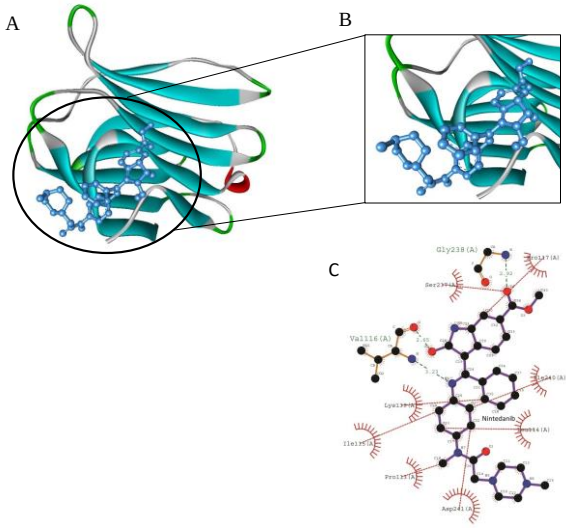
A
B
C
Nintedanib

c

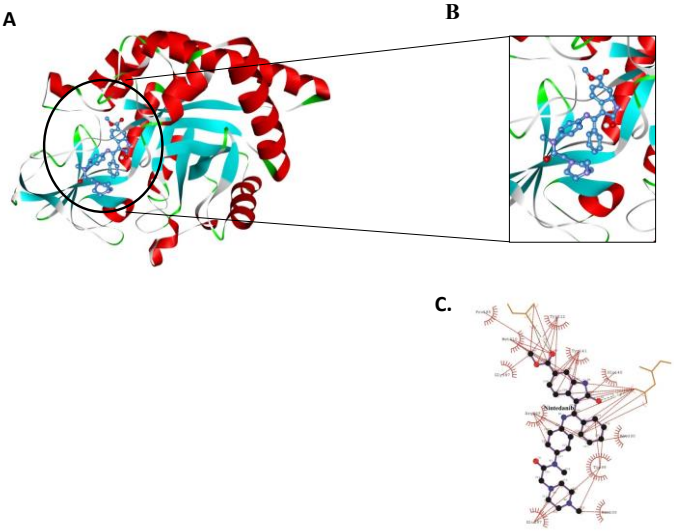
A
B
C.
Nintedanib

d

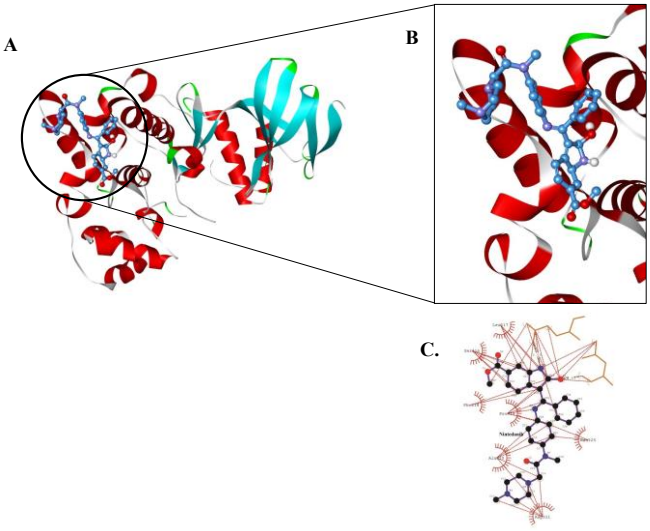
A
B
C.
Nintedanib

e

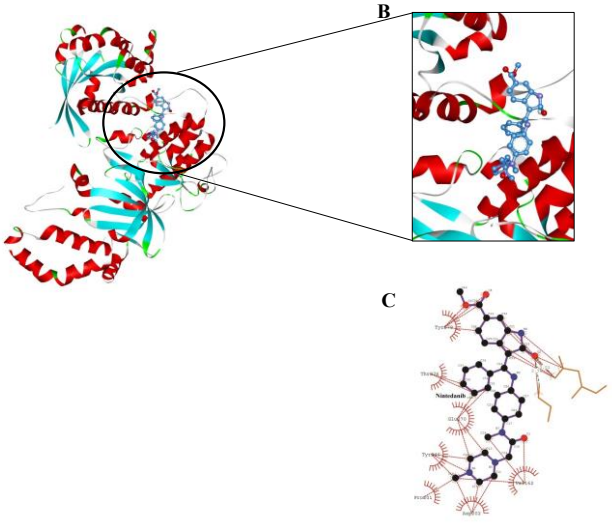
B
C
Nintedanib

f

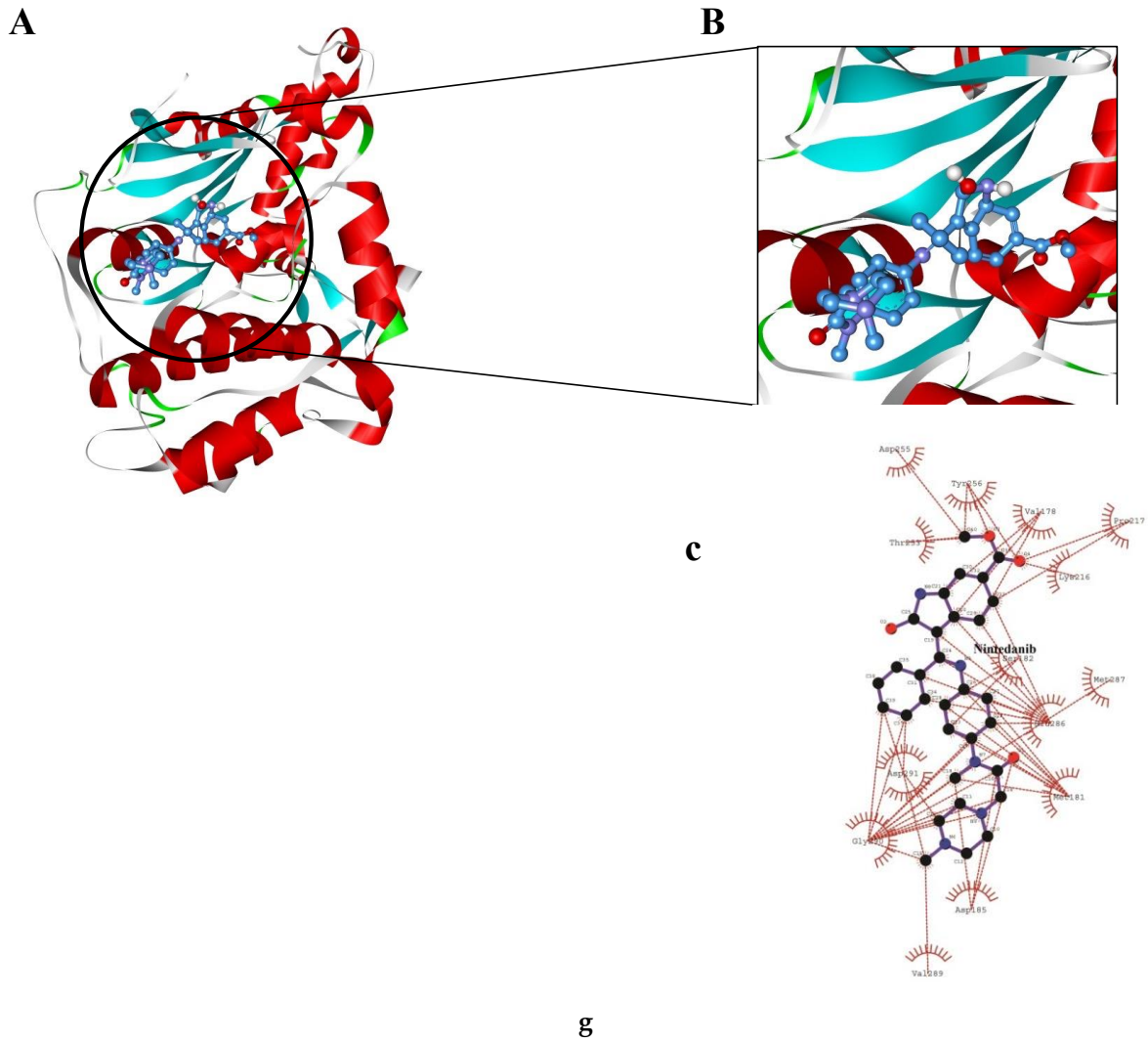

Figure 2. The binding interactions between the ligand and the different protein receptors (blind docking) of **a**: IL-13; **b**: autotaxin; **c**: Gal-3; **d**: CHIT-1; **e**: JNK; **f**: RhoE-ROCK1; and **g**: ROCK2. In each panel, **A-** represents the binding of the ligand with the receptor protein (the receptor protein is represented in the cartoon. The ligand is presented in ball stick model). **B-** represents the amino acid residues of the receptor protein binding with the ligand. **C-** represents the various types of non-covalent interactions during the binding of the ligand with the receptor.

Physiochemical and pharmacodynamics properties of the ligand

We conducted a comprehensive ADMET (absorption, distribution, metabolism, excretion, and toxicity) profile analysis for the ligand molecule (**Table X**). The ADMET study was unable to be conducted using other web servers due to limitations. SwissADME could not analyze nintedanib due to the length of its SMILES character string (exceeding 200 characters). Additionally, pkCSM was undergoing maintenance during the time of this study. Additionally, the Lipinski rule of five was applied to assess the ligand's drug-likeness properties (**Table XI**). These results indicate that nintedanib is most likely absorbed from the human intestine, has low oral bioavailability, may inhibit and be a substrate for P-glycoprotein, and is moderately toxic when administered orally in a single dose. The results indicate that the ligand possesses favorable characteristics for drug development, suggesting its potential as a promising therapeutic candidate. These results are relevant as reported by Wind *et al*.[7] previously.

Table X. List of drug-likeliness properties of nintedanib.

Parameters	Values
Molecular mass (Da)	541
Hydrogen bond donor	2
Hydrogen bond acceptors	9
LogP	2.2736
Molar refractivity (m^3/mol)	155.623642

Table XI. ADMET profile of nintedanib.

Parameters	Values
Acute oral toxicity (class)	III
Blood brain barrier	-
Human intestinal absorption	+
Human oral bioavailability	-
P-glycoprotein inhibitor	+
P-glycoprotein substrate	+

CONCLUSION

This study investigated the binding interactions of nintedanib with several ancillary proteins implicated in the pathogenesis of IPF, including RhoE-ROCK1, JNK, IL-13, Gal-3, autotaxin, and CHIT-1. Nintedanib is a well-established inhibitor of VEGFR2, PDGF, and FGFR1, which are key drivers of IPF. Our molecular docking simulations revealed that nintedanib exhibits strong binding affinities to both autotaxin and RhoE-ROCK1, comparable to its interactions with VEGFR2 and FGFR1. These findings suggest that nintedanib might exert additional beneficial effects in IPF treatment by targeting these alternative pathways. However, further in vitro studies are warranted to validate the functional implications of these binding interactions and elucidate the precise mechanisms through which nintedanib could influence IPF progression.

ACKNOWLEDGMENT

The author would like to express his gratitude to the Department of Biotechnology, Government of India, for funding this research (Grant sanction no.:BT/PR40162/BTIS/137/48/2022). The infrastructural support provided by the DBT-funded Bioinformatics and Integrative Systems Biology (BIF) Center at the University of Kalyani is also gratefully acknowledged. The author wishes to thank the University of Kalyani for its continued support.

AUTHORS' CONTRIBUTION

Conceptualization: Hari Baskar Balasubramanian, Angshuman Bagchi, Luigia Grazia Fresu, Filippo Patrucco, Piero Emilio Balbo
Data curation: Hari Baskar Balasubramanian, Angshuman Bagchi, Sima Biswas
Formal analysis: Hari Baskar Balasubramanian, Sima Biswas
Funding acquisition: -
Investigation: Hari Baskar Balasubramanian, Angshuman Bagchi, Sima Biswas
Methodology: Hari Baskar Balasubramanian, Angshuman Bagchi, Sima Biswas
Project administration: Angshuman Bagchi
Resources: Angshuman Bagchi
Software: Angshuman Bagchi, Sima Biswas
Supervision: Angshuman Bagchi, Luigia Grazia Fresu
Validation: Angshuman Bagchi
Visualization: Angshuman Bagchi, Luigia Grazia Fresu
Writing - original draft: Angshuman Bagchi, Luigia Grazia Fresu, Maria Talmon
Writing - review & editing: Hari Baskar Balasubramanian, Angshuman Bagchi, Maria Talmon

DATA AVAILABILITY

None.

CONFLICT OF INTEREST

The authors have no conflicts of interest to declare that are relevant to the content of this article.

REFERENCES

1. Phan THG, Paliogiannis P, Nasrallah GK, Giordo R, Eid AH, Fois AG, et al. Emerging cellular and molecular determinants of idiopathic pulmonary fibrosis. Cell Mol Life Sci. 2021;78(5):2031–57. DOI: 10.1007/s00018-020-03693-7; PMCID: PMC7669490; PMID: 33201251

2. Sgalla G, Iovene B, Calvello M, Ori M, Varone F, Richeldi L. Idiopathic pulmonary fibrosis: pathogenesis and management. Respir Res. 2018;19(1):32. DOI: 10.1186/s12931-018-0730-2; PMCID: PMC5824456; PMID: 29471816

3. Martinez FJ, Collard HR, Pardo A, Raghu G, Richeldi L, Selman M, et al. Idiopathic pulmonary fibrosis. Nat Rev Dis Primer. 2017;3:17074. DOI: 10.1038/nrdp.2017.74; PMID: 29052582

4. Gross TJ, Hunninghake GW. Idiopathic pulmonary fibrosis. N Engl J Med. 2001;345(7):517–25. DOI: 10.1056/nejmra003200; PMID: 11519507

5. Degryse AL, Lawson WE. Progress Toward Improving Animal Models for Idiopathic Pulmonary Fibrosis. Am J Med Sci. 2011;341(6):444–9. DOI: 10.1097/maj.0b013e31821aa000; PMCID: PMC3103078; PMID: 21613932

6. Lancaster LH, de Andrade JA, Zibrak JD, Padilla ML, Albera C, Nathan SD, et al. Pirfenidone safety and adverse event management in idiopathic pulmonary fibrosis. Eur Respir Rev. 2017;26(146):170057. DOI: 10.1183/16000617.0057-2017; PMCID: PMC9488585; PMID: 29212837

7. Wind S, Schmid U, Freiwald M, Marzin K, Lotz R, Ebner T, et al. Clinical Pharmacokinetics and Pharmacodynamics of Nintedanib. Clin Pharmacokinet. 2019;58(9):1131–47. DOI: 10.1007/s40262-019-00766-0; PMCID: PMC6719436; PMID: 31016670

8. Kolb M, Bonella F, Wollin L. Therapeutic targets in idiopathic pulmonary fibrosis. Respir Med. 2017;131:49–57. DOI: 10.1016/j.rmed.2017.07.062; PMID: 28947042

9. Li R, Jia Y, Kong X, Nie Y, Deng Y, Liu Y. Novel drug delivery systems and disease models for pulmonary fibrosis. J Controlled Release. 2022;348:95–114. DOI: 10.1016/j.jconrel.2022.05.039; PMID: 35636615

10. Hilberg F, Tontsch-Grunt U, Baum A, Le AT, Doebele RC, Lieb S, et al. Triple Angiokinase Inhibitor Nintedanib Directly Inhibits Tumor Cell Growth and Induces Tumor Shrinkage via Blocking Oncogenic Receptor Tyrosine Kinases. J Pharmacol Exp Ther. 2018;364(3):494–503. DOI: 10.1124/jpet.117.244129; PMCID: PMC6040086; PMID: 29263244

11. Swaney JS, Chapman C, Correa LD, Stebbins KJ, Bundey RA, prodanovich PC, et al. A novel, orally active LPA(1) receptor antagonist inhibits lung fibrosis in the mouse bleomycin model. Br J Pharmacol. 2010;160(7):1699–713. DOI: 10.1111/j.1476-5381.2010.00828.x; PMCID: PMC2936842; PMID: 20649573

12. Tager AM, LaCamera P, Shea BS, Campanella GS, Selman M, Zhao Z, et al. The lysophosphatidic acid receptor LPA1 links pulmonary fibrosis to lung injury by mediating fibroblast recruitment and vascular leak. Nat Med. 2008;14(1):45–54. DOI: 10.1038/nm1685; PMID: 18066075

13. Stoddard NC, Chun J. Promising pharmacological directions in the world of lysophosphatidic Acid signaling. Biomol Ther. 2015;23(1):1–11. DOI: 10.4062/biomolther.2014.109; PMCID: PMC4286743; PMID: 25593637

14. Cuozzo JW, Clark MA, Keefe AD, Kohlmann A, Mulvihill M, Ni H, et al. Novel Autotaxin Inhibitor for the Treatment of Idiopathic Pulmonary Fibrosis: A Clinical Candidate Discovered Using DNA-Encoded Chemistry. J Med Chem. 2020;63(14):7840–56. DOI: 10.1021/acs.jmedchem.0c00688; PMID: 32584034

15. Hirani N, MacKinnon AC, Nicol L, Ford P, Schambye H, Pedersen A, et al. Target inhibition of galectin-3 by inhaled TD139 in patients with idiopathic pulmonary fibrosis. Eur Respir J. 2021;57(5):2002559. DOI: 10.1183/13993003.02559-2020; PMCID: PMC8156151; PMID: 33214209

16. Shimizu Y, Dobashi K, Sano T, Yamada M. Rock Activation in Lung of Idiopathic Pulmonary Fibrosis with Oxidative Stress. Int J Immunopathol Pharmacol. 2014;27(1):37–44. DOI: 10.1177/039463201402700106; PMID: 24674677

17. Knipe RS, Tager AM, Liao JK. The Rho kinases: critical mediators of multiple profibrotic processes and rational targets for new therapies for pulmonary fibrosis. Pharmacol Rev. 2015;67(1):103–17. DOI: 10.1124/pr.114.009381; PMCID: PMC4279074; PMID: 25395505

18. Zhou Y, Huang X, Hecker L, Kurundkar D, Kurundkar A, Liu H, et al. Inhibition of mechanosensitive signaling in myofibroblasts ameliorates experimental pulmonary fibrosis. J Clin Invest. 2013;123(3):1096–108. DOI: 10.1172/jci66700; PMCID: PMC3582144; PMID: 23434591

19. Zhu Z, Homer RJ, Wang Z, Chen Q, Geba GP, Wang J, et al. Pulmonary expression of interleukin-13 causes inflammation, mucus hypersecretion, subepithelial fibrosis, physiologic abnormalities, and eotaxin production. J Clin Invest. 1999;103(6):779–88. DOI: 10.1172/jci5909; PMCID: PMC408149; PMID: 10079098

20. Castro M, Corren J, Pavord ID, Maspero J, Wenzel S, Rabe KF, et al. Dupilumab Efficacy and Safety in Moderate-to-Severe Uncontrolled Asthma. N Engl J Med. 2018;378(26):2486–96. DOI: 10.1056/nejmoa1804092; PMID: 29782217

21. Panettieri Jr RA, Sjöbring U, Péterffy A, Wessman P, Bowen K, Piper E, et al. Tralokinumab for severe, uncontrolled asthma (STRATOS 1 and STRATOS 2): two randomised, double-blind, placebo-controlled, phase 3 clinical trials. Lancet Respir Med. 2018;6(7):511–25. DOI: 10.1016/s2213-2600(18)30184-x; PMID: 29792288

22. Hanania NA, Korenblat P, Chapman KR, Bateman ED, Kopecky P, Paggiaro P, et al. Efficacy and safety of lebrikizumab in patients with uncontrolled asthma (LAVOLTA I and LAVOLTA II): replicate, phase 3, randomised, double-blind, placebo-controlled trials. Lancet Respir Med. 2016;4(10):781–96. DOI: 10.1016/s2213-2600(16)30265-x; PMID: 27616196

23. Maher TM, van der Aar EM, Van de Steen O, Allamassey L, Desrivot J, Dupont S, et al. Safety, tolerability, pharmacokinetics, and pharmacodynamics of GLPG1690, a novel autotaxin inhibitor, to treat idiopathic pulmonary fibrosis (FLORA): a phase 2a randomised placebo-controlled trial. Lancet Respir Med. 2018;6(8):627–35. DOI: 10.1016/s2213-2600(18)30181-4; PMID: 29792287

24. Di Rosa M, Malaguarnera L. Chitotriosidase: A New Inflammatory Marker in Diabetic Complications. Pathobiology. 2016;83(4):211–9. DOI: 10.1159/000443932; PMID: 27116685

25. Koralewski R, Dymek B, Mazur M, Sklepkiewicz P, Olejniczak S, Czestkowski W, et al. Discovery of OATD-01, a First-in-Class Chitinase Inhibitor as Potential New Therapeutics for Idiopathic Pulmonary Fibrosis. J Med Chem. 2020;63(24):15527–40. DOI: 10.1021/acs.jmedchem.0c01179; PMID: 33078933

26. Sklepkiewicz P, Dymek BA, Mlacki M, Koralewski R, Mazur M, Nejman-Gryz P, et al. Inhibition of CHIT1 as a novel therapeutic approach in idiopathic pulmonary fibrosis. Eur J Pharmacol. 2022;919:174792. DOI: 10.1016/j.ejphar.2022.174792; PMID: 35122869

27. Alcorn JF, van der Velden J, Brown AL, McElhinney B, Irvin CG, Janssen-Heininger YMWJ. c-Jun N-Terminal Kinase 1 Is Required for the Development of Pulmonary Fibrosis. Am J Respir Cell Mol Biol. 2009;40(4):422–32. DOI: 10.1165/rcmb.2008-0174oc; PMCID: PMC2660560; PMID: 18836136

28. Bennett BL. c-Jun N-terminal kinase-dependent mechanisms in respiratory disease. Eur Respir J. 2006;28(3):651–61. DOI: 10.1183/09031936.06.00012106; PMID: 16946096

29. Lee VY, Schroedl C, Brunelle JK, Buccellato LJ, Akinci OI, Kaneto H, et al. Bleomycin induces alveolar epithelial cell death through JNK-dependent activation of the mitochondrial death pathway. Am J Physiol Lung Cell Mol Physiol. 2005;289(4):L521–8. DOI: 10.1152/ajplung.00340.2004; PMID: 16148050

30. Lin CH, Yu MC, Tung WH, Chen TT, et al. Connective tissue growth factor induces collagen I expression in human lung fibroblasts through the Rac1/MLK3/JNK/AP-1 pathway. Biochim Biophys Acta. 2013;1833(12):2823–33. DOI: 10.1016/j.bbamcr.2013.07.016; PMID: 23906792

31. Baroroh U, Muscifa ZS, Destiarani W, Rohmatullah FG, Yusuf M. Molecular interaction analysis and visualization of protein-ligand docking using Biovia Discovery Studio Visualizer. Indones J Comput Biol. 2023;2(1):22-30. DOI: 10.24198/ijcb.v2i1.46322

32. Agu PC, Afiukwa CA, Orji OU, Ezeh EM, Ofoke IH, Ogbu CO, et al. Molecular docking as a tool for the discovery of molecular targets of nutraceuticals in diseases management. Sci Rep. 2023;13(1):13398. DOI: 10.1038/s41598-023-40160-2; PMCID: PMC10435576; PMID: 37592012

33. Yang J, Roy A, Zhang Y. Protein-ligand binding site recognition using complementary binding-specific substructure comparison and sequence profile alignment. Bioinformatics. 2013;29(20):2588-95. DOI: 10.1093/bioinformatics/btt447; PMCID: PMC3789548; PMID: 23975762

34. Meng XY, Zhang HX, Mezei M, Cui M. Molecular docking: a powerful approach for structure-based drug discovery. Curr Compout Aided Drug Des. 2011;7(2):146-57. DOI: 10.2174/157340911795677602; PMCID: PMC3151162; PMID: 21534921

35. Fu Y, Zhao J, Chen Z. Insights into the Molecular Mechanisms of Protein-Ligand Interactions by Molecular Docking and Molecular Dynamics Simulation: A Case of Oligopeptide Binding Protein. Comput Math Methods Med. 2018;2018:3502514. DOI: 10.1155/2018/3502514; PMCID: PMC6305025; PMID: 30627209

36. Zhang W, Bell EW, Yin M, Zhang Y. EDock: blind protein-ligand docking by replica-exchange monte carlo simulation. J Cheminform. 2020;12(1):37. DOI: 10.1186/s13321-020-00440-9; PMCID: PMC7251717; PMID: 33430966